Laser Photonics Rev. **5**, No. 5, 659–676 (2011) / **DOI** 10.1002/lpor.201000044

LASER & PHOTONICS REVIEWS

Abstract This paper gives an overview of the results obtained with diode-pumped Neodymium-doped crystals operating below 900 nm. Operation at such low wavelengths requires considering the strong thermal population of the lower level of the laser transition. Based on a theoretical study and simulations, the paper presents the challenges related to the design of these three-level lasers. Experimental results are given with Nd:YAG and Nd:vanadate crystals. It is explained how to deal with the line competition with emission at 946 nm or 912 nm. Finally, intracavity second-harmonic generation is presented. The output powers reach a few hundred mW at wavelengths below 450 nm. Hence, the paper demonstrates the potential of Nd-doped diode-pumped solid-state lasers for applications in the blue range, in replacement of gas lasers such as helium-cadmium lasers.

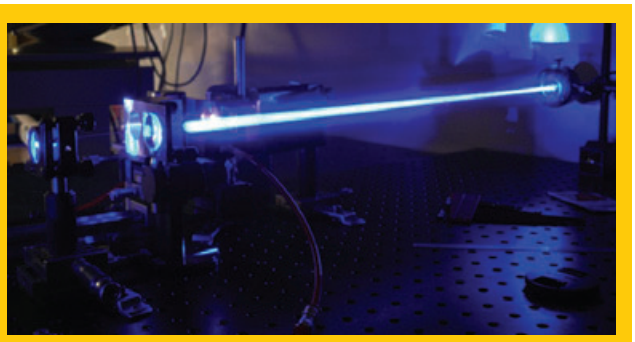

Low-wavelength emission of Nd-doped lasers

François Balembois[*], **Marc Castaing, Emilie Hérault, and Patrick Georges**

1. Introduction

As a "light concentrate", the laser has driven a large range of applications, especially in the blue part of the visible spectrum. Generally, a laser beam can be focused on a diameter of the order of the wavelength, this means a diameter around 400 nm for the blue range. This property is widely used for applications such that data storage, compact disc mastering, flow visualization or cytometry, where the size of the illuminated objects is very small. As "spectral concentrate", blue-laser sources are also used for holography or Raman spectroscopy. Moreover, blue wavelengths are absorbed by numerous biological species. Blue lasers are often used as excitation sources for fluorescence microscopy.

During more than two decades, the only laser sources used in this range were gas lasers: argon lasers (emission at 488 nm, for example) or helium-cadmium lasers (emission at 442 nm, for example). The drawbacks of these sources are numerous: very low efficiency associated with high power consumption, cumbersome cooling and driving systems, moderate lifetime and needs for regular maintenance. These inconveniences acted as a brake for the development of applications asking for high integration level or portability. Even if the blue laser requirements are fully understood by laser scientists, the development of compact laser sources with high spatial and spectral quality beams is not that obvious. The main point is that laser media emitting directly in the blue spectral range are very rare: gas and more recently gallium nitride semiconductors [1] are the only ones. Much hope has been put on these semiconductor materials that are now widely used for DVD. Indeed, semiconductor lasers are the most compact and efficient lasers ever developed with a volume of a few mm^3 and a typical wall plug efficiency of 50%. However, they can not address all the requirements for blue-laser sources, since their power is limited, their beam quality is degraded at high power level, (above 100 mW typically in the blue) and their spectral width is larger than 1 nm, limiting the coherence length and their interest for interferometry experiments.

An indirect way is to use frequency conversion of laser sources emitting in the near-infrared with nonlinear crystals. The first idea is to frequency-double high-power laser diodes emitting in the range 800–980 nm. Indeed, nearly all the studies have been concentrated on the 976 nm for the replacement of argon lasers. Output power up to the watt level has been obtained at 488 nm with single-mode laser diodes coupled with efficient nonlinear crystals (periodically poled lithium niobates) and waveguides [2, 3]. Even if the derivation of this concept is possible at other wavelengths, it has never been demonstrated for blue emission below 488 nm.

Indeed, the blue range can be separated in two bands: from 400 nm to 450 nm and from 450 nm to 500 nm. As far as the second-harmonic conversion process is concerned, the fundamental wavelengths can also be separated in two bands: from 800 nm to 900 nm and from 900 nm to 1000 nm.

The latter has been addressed for years by neodymium-doped crystals pumped by laser diodes: for example emission at 946 nm for Nd:YAG or 914 nm for Nd:YVO_4 [4–6]. More recently, ytterbium-doped materials (crystals or glass fibres) have been used for the replacement of the argon line at 488 nm (976 nm [7, 8] emission followed by frequency doubling [9–12]). The wavelengths emitted by Nd-doped and Yb-doped materials are fixed by the interaction between the ions and the host. This leads generally to spectral bandwidths of a few nanometers at a maximum. Some more flexibility can be obtained with semiconductors since the band-

Laboratoire Charles Fabry de l'Institut d'Optique, CNRS, Univ Paris-Sud, Campus Polytechnique, RD128, 91127 Palaiseau Cedex, France
[*] Corresponding author: e-mail: francois.balembois@institutoptique.fr

widths are generally a few tens of nanometers broad. The optically pumped semiconductors (OPS) [13] can provide high beam quality and high output power at wavelengths that are not covered by laser crystals. An impressive output power of 15 W has been demonstrated at 488 nm by second-harmonic generation [14]. Commercial products based on OPS can provide laser emission at 460 nm or 488 nm [15]. It is worth noting that OPS are diode pumped, generally around 800 nm. This provides the compactness, efficiency and reliability expected for laser sources integrated in devices.

The 800–900 nm band could be covered by metal transition ions such as Ti^{3+} or Cr^{3+} in different host materials (sapphire for the Ti^{3+} [16] or colquiriites such as LiSAF for the Cr^{3+} [17]). The advantage is that this range can be continuously covered since the emission is broadened to more than 100 nm by vibronic interactions. Tunable blue light has been demonstrated with Ti:sapphire or Cr:LiSAF [18–21]. However, the problem comes from the pumping wavelength: the absorption bands are shifted in the visible, in comparison to lasers emitting between 900 nm and 1000 nm. Hence, Ti:sapphire is often pumped in the green (532 nm) by frequency-doubled Nd-doped lasers. Even though those lasers are well known, with commercial versions available for more than ten years, they are complex and costly. Direct diode pumping could be preferred for its simplicity. However, no high-power laser diode exists in the green to pump the Ti:sapphire. There is only the very recent demonstration of a Ti:sapphire pumped by a blue laser diode at 445 nm [22]. The case of Cr:LiSAF is more favorable since it can be diode pumped at 670 nm. However, Cr:LiSAF suffers from important thermal problems that are difficult to manage and that limit dramatically the output power [23].

Pumping in the red is also possible for appropriate optically pumped semiconductors: laser emission in the range of 100 mW has already been demonstrated at 852 nm with a diode-pumping at 690 nm [24]. However, the red pump laser diodes are not as good and as efficient as near-infrared laser diodes. Over the years, the progress in red laser diode performance has been very small compared to the laser diodes in the range 800–980 nm, improving continuously their brightness, power and even efficiency. In addition, optically pumped semiconductors are not yet optimized for wavelength below 900 nm. As an example, operating photodegradations of semiconductor layers have been observed at 880 nm [25]. Finally, solid-state lasers pumped by red laser diodes and emitting in the band 800–900 nm require technological effort for the development of efficient semiconductors.

Let us tackle the problem of laser sources between 800 nm and 900 nm from another point of view. The efficiency and compactness of laser sources are primarily related to the pump. As 800-nm laser diodes are much more efficient than their red counterparts, let us consider them as the pump source. A pump wavelength around 800 nm leads naturally to consider Nd-doped materials. Indeed, the impressive development of semiconductors around 800 nm is precisely driven by this application of pumping. Following this approach, laser scientists have designed a cascade of nonlinear processes to reach the right wavelength in the blue with 808-nm pumped Nd:YAG or Nd:YVO_4 lasers. Fundamental laser emission was achieved at 1319 nm and 1342 nm, respectively. Emissions at 440 nm and 447 nm were realized after two stages of nonlinear crystals [26, 27]: the first one for frequency doubling and the second one for sum-frequency mixing. Even if a few hundred milliwatts have been produced in Q-switched operation, a blue power of only 3 mW is obtained in continuous wave at 440 nm [27]. The two stages of nonlinear conversion reduce the overall efficiency and increase the complexity compared to second-harmonic generation.

From a more general point of view, let us recall that the laser emission is always higher than the pump wavelength (except for up-conversion lasers, which are generally not easy to operate because of complex energy-level schemes, as Dy:ZBLAN, for example [28]). This means that it should be possible to operate below 900 nm with pumping at 800 nm and to obtain blue emission below 450 nm by a simple process of frequency doubling. The key point is to find the gain medium. Generally, the lowest laser wavelength achieved with Nd-doped media corresponds to laser emission between the $^4F_{3/2}$ emitting level and the highest sublevel of the $^4I_{9/2}$ manifold. This leads to the well-known 946-nm emission in Nd:YAG or to 914 nm in Nd:YVO_4. The first question would be: are there other materials with a larger gap between the $^4F_{3/2}$ and the $^4I_{9/2}$ in order to achieve laser emission at lower wavelength, closer to 900 nm or even below? As an example, Nd:YLF presents lines at 903 nm and 908 nm that were demonstrated in 2000 [29]. Efficient second-harmonic generation at 454 nm was reported ten years later with a blue power of more than 4 watts [30]. At lower wavelength, Nd:ASL has demonstrated laser emission at 901 nm [31]. Under diode pumping, a frequency-doubled Nd:ASL produced 53 mW at 453 nm [32]. Some experiments have also been carried out in order to identify new laser hosts with the largest splitting possible between the $^4F_{3/2}$ and the $^4I_{9/2}$. Scheelite-type structure can be mentioned with, for example, Nd:$BaWO_4$ [33].

The second question would be: is it possible to obtain a laser effect in Nd-doped media with a lower level of the laser transition closest to the ground state? As an example, Nd:YAG spontaneous emission was observed at lower wavelengths than 946 nm in 1972 [34] (namely 900 nm and 891 nm), involving lower sublevels of the $^4I_{9/2}$ manifold (Fig. 1). Laser emission is also observed in Nd:$LiNbO_3$ waveguides at 889 nm [35]. The answer to this question is the purpose of this paper.

In Sect. 2, we explain how we can chose the gain media, the subject of the study been restricted to the most efficient Nd-doped crystals. As the lower level of the considered transition will be strongly thermally populated, Sect. 3 gives specific guidelines for the laser development. This section is based on a theoretical approach and on simulation of the laser power as a function of different parameters such as the crystal length, the beam sizes and the pump brightness. The next section (4) presents the results obtained on two crystals: Nd:YAG (for laser emission at 900 nm, 884nm and even 869 nm) and vanadate crystals (for laser emission at

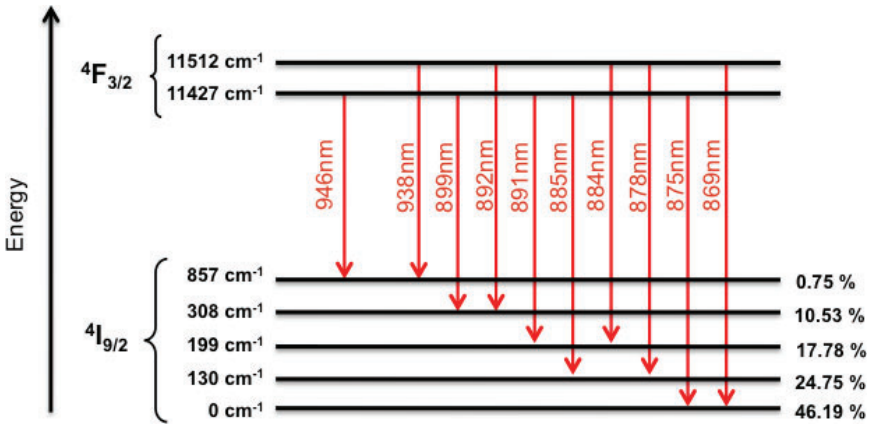

Figure 1 (online color at: www.lpr-journal.org) Energy levels of Nd:YAG and possible emission wavelengths. On the right, fraction of the $^4I_{9/2}$ population following the different sublevels.

879 nm and 880 nm). Section 5 describes the realization of intracavity frequency doubling of these lasers in order to reach blue emission below 450 nm. The last section (6) discusses the performance obtained in comparison to other sources and concludes on the potential of Nd-doped lasers emitting at low wavelengths.

2. Choice of Nd-doped crystals for laser emission at low wavelength

The first quantity to be considered in order to achieve laser emission is the gain coefficient g. It is related to the effective cross sections at the laser wavelength (absorption cross section σ_{al} and emission cross section σ_{el}) and to the population densities of the upper manifold $^4F_{3/2}$ (n_2) and of the lower manifold $^4I_{9/2}$ (n_1). The relation is given by

$$g = \sigma_{el} n_2 - \sigma_{al} n_1 \,. \tag{1}$$

Following the definition of the effective cross sections, the higher effective absorption cross section, the more populated the lower level of the laser transition. A large population density in the upper level is needed to have a positive gain coefficient. Consequently, it is important to select Nd-doped materials with high fluorescence quantum efficiencies in order to avoid leakage of population from the upper level by nonradiative effects. This simple remark excludes the use of borate crystals such that Nd:YAB, Nd:YCOB or Nd:GdCOB, despite their interesting self-frequency-doubling properties: their quantum efficiencies stay between 15% and 26% [36, 37] because of high-energy phonons and high relaxation multiphonon rate.

Under steady state and with a continuous pumping, the gain coefficient can be written as follows with the pump parameters and the spectroscopic data of the crystal:

$$g = n_t \frac{\sigma_{el}.\sigma_{ap}.I_p \frac{\lambda_p}{hc} - \frac{\sigma_{al}}{\tau}}{\sigma_{ap}.I_p \frac{\lambda_p}{hc} + (\sigma_{al} + \sigma_{el}).I.\frac{\lambda}{hc} + \frac{1}{\tau}} \tag{2}$$

where $n_t = n_1 + n_2$ is the total population density of Nd ions in the medium, σ_{ap} is the absorption cross section, I_p is the pump intensity (in W/cm^2), λ_p is the pump wavelength, h is the Planck constant, c is the speed of light in vacuum, τ is the lifetime of the $^4F_{3/2}$ level, I is the laser intensity, and λ the laser wavelength. g, I and I_p are considered at the same point of the crystal. In the general case, the lifetime decreases with the concentration in Nd ions (i.e. n_t) because of nonradiative processes. However, in this study, we consider low-doped crystals such that this effect can be neglected.

Without pumping, the gain is negative (absorption). It starts to be positive if the pump intensity reaches a particular value defined as the pump transparency intensity I_{ptr}:

$$I_{ptr} = \frac{hc}{\lambda_p} \frac{\sigma_{al}}{\sigma_{ap}.\sigma_{el}}.\frac{1}{\tau} \tag{3}$$

In Eq. (3), the absorption cross section at the pump wavelength σ_{ap} appears. For a Nd medium, the absorption around 800 nm generally consists of peaks with a narrow linewidth of a few nanometers. As high-power laser diodes around 800 nm could have typical spectral widths between 2 nm to 3 nm, the absorption cross section in not constant for all the spectral components of the laser diode. Therefore, one has to use an averaged value of the absorption cross section denoted $\overline{\sigma_{ap}}$ expressed by Eq. (4) assuming a gaussian spectral shape for the laser diode.

$$\overline{\sigma_{ap}} = \int_{\lambda_p - 2\Delta\lambda_p}^{\lambda_p + 2\Delta\lambda_p} \sigma_{ap}(\lambda).\frac{\exp - \left[\frac{1}{2}.\left(\frac{\lambda - \lambda_p}{2\Delta\lambda_p\sqrt{2\ln 2}}\right)^2\right]}{2\Delta\lambda_p\sqrt{4\pi\ln 2}}.d\lambda \tag{4}$$

where λ_p is the peak of the pump spectrum and $\Delta\lambda_p$ is the spectral width (full width at half-maximum, FWHM) of the laser diode spectrum. The new average value for the pump transparency intensity can then be expressed by:

$$\overline{I_{ptr}} = \frac{hc}{\lambda_p} \frac{\sigma_{al}}{(\overline{\sigma_{ap}}).\sigma_{el}}.\frac{1}{\tau} \tag{5}$$

We have calculated $\overline{\sigma_{ap}}$ for three different crystals: Nd:YAG, Nd:YVO_4 and Nd:$GdVO_4$ around 808 nm taking the spectral width (FWHM) of the laser diode at $\Delta\lambda_p = 2$ nm. We found a ratio $\overline{\sigma_{ap}}/\sigma_{ap}$ of approximately 0.6 for the these three crystals. Consequently, the spectral broadness of the high-power laser diodes leads to an increase of the transparency intensity of more than 1.6, following Eq. (5) in

Table 1 Average transparency intensity and related data for different Nd-doped crystals at selected wavelengths below 900 nm. Data for Nd:YAG, Nd:YVO_4 and Nd:$GdVO_4$ from [38], [39] and [40], respectively. For the vanadate, the laser effect is always considered on the π polarization.

Host	$\overline{\sigma_{ap}}$ (cm^2)	Lifetime τ (µs)	Wavelength	σ_{al} (cm^2)	σ_{el} (cm^2)	$\overline{I_{ptr}}$ (kW/cm^2)
YAG	4.8×10^{-20}	230	899 nm	1.5×10^{-21}	8×10^{-21}	4.2
YAG	4.8×10^{-20}	230	884 nm	10^{-20}	1.7×10^{-20}	13.1
YAG	4.8×10^{-20}	230	869 nm	1.7×10^{-20}	1.1×10^{-20}	34.4
YVO_4 (π)	3.6×10^{-19}	100	880 nm	4.3×10^{-19}	8.6×10^{-20}	33.8
YVO_4 (σ)	8.1×10^{-20}	100	880 nm	$4.3\times10^{-19}(\pi)$	$8.6\times10^{-20}(\pi)$	151.9
$GdVO_4$ (π)	3.5×10^{-19}	100	879 nm	2.8×10^{-19}	1.9×10^{-19}	10.4
$GdVO_4$ (σ)	8.5×10^{-20}	100	879 nm	$2.8\times10^{-19}(\pi)$	$1.9\times10^{-19}(\pi)$	42.6

comparison with a monochromatic pump source (such as a Ti:sapphire for example).

Table 1 gives the different data used for the calculation of $\overline{I_{ptr}}$ for different crystals from [38–40]. Let us consider the Nd:YAG as a first example. For the legibility of the table, only several wavelengths have been selected among all the possibilities presented in Fig. 1. As expected, the lower the emission wavelength, the higher is the pump transparency. Table 1 shows that it is possible to operate below 900 nm at moderate pump transparency (below a few tens of kW/cm^2). As an example, the intensity on the output of a fiber-coupled laser diode emitting 20 W in a 200-µm core fiber corresponds to 63.7 kW/cm^2. Moreover, the very low pump transparency at 899 nm is particularly interesting and experimental results on this laser line will be given in Sect. 4 and in Sect. 5.

Let us now study the potential of Nd-doped media for laser operation on a pure three-level transition, the lower level being the fundamental level. The corresponding wavelengths are 869 nm for Nd:YAG, 880 nm for Nd:YVO_4 and 879 nm for Nd:$GdVO_4$. As the absorption is polarization dependent for the vanadate crystals, we calculate the transparency intensity for polarization π and σ. The transparency intensities are here much higher than at 899 nm for Nd:YAG. It is worth noting the relatively low value for the Nd:$GdVO_4$ on the π polarization. Experimental results will be presented on this crystal in Sect. 4 and in Sect. 5.

Finally, this section shows that laser operation is possible below 900 nm with classical Nd-doped crystals because I_{ptr} is lower than the intensity that could be obtained at the focus of "a state-of-the-art" laser diode pump beam. This section also shows that the pump transparency is strongly dependent on the pump-source characteristics: pump polarization and spectrum are two parameters that increase this value significantly.

However, reaching the pump transparency at the focus point in the gain medium is not enough. One has to consider the entire length of the crystal and particularly the end of the crystal where reabsorption may occur, in the case of one-side longitudinal pumping.

From a more general point of view, one has to take in account the different parameters for the laser design in the very specific case of a diode pumped three-level laser. This is the purpose of the next section.

3. Guidelines for the laser development of a diode-pumped three-level laser

Let us recall that our goal is to investigate laser emission below 900 nm in Nd:doped crystals on the way to produce blue light by second-harmonic generation. As this nonlinear process requires high intensity in the fundamental wavelength, one classical way is to put the frequency converter directly inside the cavity where the intensity is generally much higher than after an output coupler. Consequently, the intracavity power is an important parameter to investigate the potential of a Nd-doped crystal below 900 nm. This is the parameter chosen for the laser development. Below 900 nm, a Nd-doped laser can be a quasi-three-level laser or a three-level laser. As seen in the previous part with the pump transparency, a three-level laser is more complicated to develop than a quasi-three-level one. Therefore, we propose to focus the study only on three-level systems (even if the theory presented here could be applied on a quasi-three-level laser). We propose to give numerical examples based on Nd:$GdVO_4$ since it has a low pump transparency (Table 1).

In the first section (3.1), we explain how the intracavity power can be calculated. In the second section (3.2), we present how the intracavity power varies with different parameters needed for the laser design. In order to understand where the difficulties are, we compare the performance of a pure three-level system with the one calculated for a four-level system having the same parameters. In the last section (3.3), we discuss the importance of the optimization criteria and present one way to make a three-level system more tolerant.

3.1. Theoretical approach

The three-level laser is schematically represented in Fig. 2 for the simulations. We supposed a longitudinal pumping

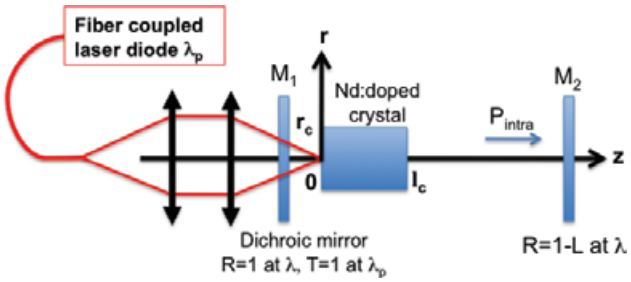

Figure 2 (online color at: www.lpr-journal.org) Basic laser scheme used for the simulation.

coming from a fiber coupled laser diode. The modelling of longitudinally pumped quasi-three-level lasers has been carried out by many authors [41–44] but they are not completely adapted to the modelization of a Nd-doped laser operating at low wavelengths since depletion of the ground state is generally not taken in account. However, this effect will have a strong influence on the laser action since a strong population in the upper level is needed to achieved the transparency of the medium. Our model is close to the one developed by Yiou et al [45] but adapted in the case of low loss cavities, since the purpose of this paper is intracavity second-harmonic generation. In order to be complete, we give all the steps of the model in this section.

Both pump and laser are supposed to run in continuous wave. The cylindrical symmetry of the setup allows simplifying the problem with only two coordinates: z, on the propagation axis and r perpendicular to the propagation axis. The first mirror is a dichroic mirror perfectly transparent for the pump beam and perfectly reflective for the laser beam. We suppose for simplicity that all the cavity losses (denoted L) are concentrated on the second mirror. Hence, this mirror has a transmission of L. For efficient intracavity second-harmonic generation, we need to design a low-loss cavity. This means that the laser intensity circulating in one direction is very close to the intensity in the other direction. Therefore, the gain G in one direction is very close to the gain in the other one. When the laser is running under the steady state, we can then write that:

$$G^2(1-L)=1\,. \tag{6}$$

The purpose of the following equations is to relate the gain G to the other laser parameters (beam sizes, intensities, etc.).

The pump beam is described by a Gaussian law in transverse section (Eqs. (7) and (8)), while beam propagation along the z direction takes into account the pump beam M^2 factor (Eq. (9)). This beam profile has been experimentally observed in the vicinity of the focus point for the laser diodes used in the different setups presented in Sect. 4.

The pump intensity in the gain medium is given by,

$$I_\mathrm{p}(r,z)=I_\mathrm{p}(0,z).e^{-\frac{2r^2}{w_\mathrm{p}^2(z)}} \tag{7}$$

with

$$I_\mathrm{p}(0,0)=\frac{2.P_\mathrm{p}}{\pi.w_\mathrm{p}^2(0)}\,, \tag{8}$$

P_p being the incident pump power on the Nd-doped crystal, and

$$w_\mathrm{p}^2(z)=w_{p0}\sqrt{1+\left(M^2.\frac{\lambda_\mathrm{p}}{\pi.n.w_{p0}^2}(z-z_{p0})\right)^2}\,. \tag{9}$$

n is the refractive index of the crystal, z_{p0} is the position of the pump focus in the crystal, w_{p0} is the pump radius at the focus in the crystal and M^2 represents the beam quality of the pump beam. M^2 is calculated from the parameters of the fiber of the pump laser diode.

$$M^2=\frac{\arcsin(\mathrm{NA}).\pi.\frac{\Phi_\mathrm{core}}{2}}{\lambda_\mathrm{p}}\,. \tag{10}$$

NA is the numerical aperture of the pump fiber and Φ_core is its diameter. Note that the relation between Φ_core and w_{p0} depends on the magnification of the pump optics (see Fig. 2). This relation is not needed at this stage of the calculation.

The pump intensity on the propagation axis $I_\mathrm{p}(0,z)$ is described by the following equation:

$$\frac{dI_\mathrm{p}(0,z)}{dz}=-I_\mathrm{p}(0,z).n_\mathrm{t}.\sigma_\mathrm{ap} \times\frac{\sigma_\mathrm{el}.I(0,z)\frac{\lambda}{hc}+\frac{1}{\tau}}{\sigma_\mathrm{ap}.I_\mathrm{p}(0,z)\frac{\lambda_\mathrm{p}}{hc}+(\sigma_\mathrm{al}+\sigma_\mathrm{el}).I(0,z).\frac{\lambda}{hc}+\frac{1}{\tau}}\,. \tag{11}$$

$I(0,z)$ is the total intensity of the laser on the propagation axis and inside the cavity, including the two counterpropagating laser beams.

The laser beam transverse distribution is considered to be close to the TEM_{00} fundamental mode Gaussian distribution, with beam quality characterized by $M^2=1$ and the intensity in each point is:

$$I(r,z)=\frac{2.P_\mathrm{total}}{\pi.w^2(z)}.e^{-\frac{2r^2}{w^2(z)}}\,, \tag{12}$$

where

$$w^2(z)=w_0\sqrt{1+\left(\frac{\lambda}{\pi.n.w_0^2}(z-z_0)\right)^2}\,, \tag{13}$$

P_total is the total power illuminating each slice of crystal perpendicular to the cavity axis, w_0 is the beam radius in the waist plane and z_0 is the distance of the waist plane from the crystal input.

As the laser consists in a linear cavity, two signal beams propagating in opposite directions illuminate each crystal slice. The low value of the cavity losses also implies that the gain medium is strongly saturated. Under these conditions, the effect of interferences between the signal beam on the population inversion can be neglected. Therefore, P_total can be related to P_intra, the signal power circulating from the left to the right in the cavity by:

$$P_\mathrm{total}=P_\mathrm{intra}+P_\mathrm{intra}(1-L)\,. \tag{14}$$

Finally, the gain can be related to other laser parameters by:

$$G = Exp\left(4\int_{z=0}^{z=l_c}\cdot\int_{r=0}^{r=r_c}\frac{g(r,z)}{w^2(z)}\cdot\exp\left(-\frac{2r^2}{w^2(z)}\right)rdr.dz\right), \quad (15)$$

$g(r,z)$ being the small-signal gain coefficient given by Eq. (2).

The simulation starts from a set of data describing the laser:

- the crystal, with its refractive index n, its length l_c and all its cross sections,
- the pump beam with P_p, NA and Φ_{core}, w_{p0} and z_{p0},
- the cavity with w_0 , z_0, and the cavity losses L.

The core of the calculations is the knowledge of the two functions describing the intensities: $I_p(r,z)$ and $I(r,z)$ needed to calculate the gain coefficient g (Eq. (2)) and the gain G (Eq. (15)). Note from Eq. (11) that $I_p(0,z)$ could be more complicated than the classical exponential decrease function because of gain saturation. The goal of the calculation is to find a value of P_{intra} such that Eq. (6) is fulfilled, meaning that the laser runs under steady state. The numerical program we have developed is based on a feedback loop. Starting from a given value of P_{intra}, the functions $I_p(r,z)$ and $I(r,z)$ are determined and the gain G is calculated. The quantity $G^2(1-L)$ is then compared to 1: $G^2(1-L) > 1$ means that the gain is not saturated enough by P_{intra} and that P_{intra} must be increased. On the other hand, $G^2(1-L) < 1$ means that P_{intra} must be decreased. By a dichotomy convergence, the calculation finally gives the intracavity power P_{intra} for the set of parameters given above.

3.2. Evolution of the intracavity power with the laser parameters

In order to be more concrete, we took the example of a Nd:$GdVO_4$ crystal with a length $l_c = 5$ mm and a doping concentration of 0.1%. We supposed that the laser operates at 879 nm with pumping at 808 nm. The results of simulations for this three-level laser are systematically compared with an imaginary four-level laser having the same parameters as Nd:$GdVO_4$ operating at 879 nm except for the absorption cross section at the lasing wavelength (set at $\sigma_{al} = 0$). The set of parameters used in this section (and also Sect. 3.3) is: $P_p = 20$ W, NA $= 0.22$, $M^2 = 43$, $w_{p0} = 100\,\mu$m, $z_{p0} = 1.66$ mm, $w_0 = 55\,\mu$m, $z_0 = 0$ mm, $L = 3\%$. It corresponds to some of the experimental conditions that will be presented in Sects. 4 and 5.

First, we investigate the influence of the signal beam size on the intracavity power (Fig. 3). The first noteworthy fact is that P_{intra} is much larger in a four-level laser than in a three-level laser. This is related to the high population level of the ground state: a significant part of the pump power is used to reach the transparency of the medium in the three-level laser, whereas the total pump power is used for laser action in the four-level system. Figure 3 shows that the beam size w_0 must be chosen carefully in the case of a three-level laser: if it is too small, the overlap between the pump beam and the cavity beam is strongly reduced,

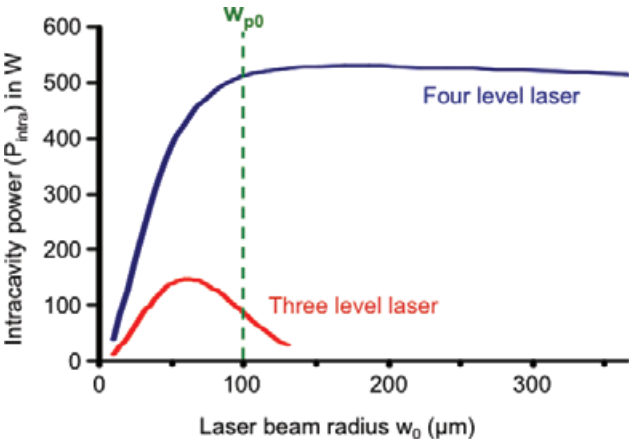

Figure 3 (online color at: www.lpr-journal.org) Evolution of the intracavity power P_{intra} versus the laser beam radius w_0. The three-level laser refers to Nd:GVO_4, the four-level laser refers to an imaginary laser with $\sigma_{al} = 0$.

limiting the gain and the intracavity power. If w_0 is too large, parts of the cavity beam are in zones where the pump transparency is not reached, as the pump intensity is not constant in a transverse plane (see Eq. (7)). This induces reabsorption losses and gain limitation. The optimization of P_{intra} requires to take a beam size w_0 much smaller than the pump size (nearly a factor of 2 in our case). Consequently, the overlap between the pump beam and the cavity beam is intrinsically limited by this requirement. Note that this effect does not occur on the four-level laser where the condition $w_0 >= w_{p0}$ has simply to be fulfilled.

As the overlap between the pump beam and the cavity beam is problematic in a three-level laser, we investigated the effect of the pump-beam quality (M^2) on the intracavity power. Figure 4 shows that the three-level laser is very dependent on this parameter, with a linear decrease. Physically, a pump beam with a poor quality increases the volume where the pump transparency is not reached and reduces the gain consequently. The shape of the curve for a four-level

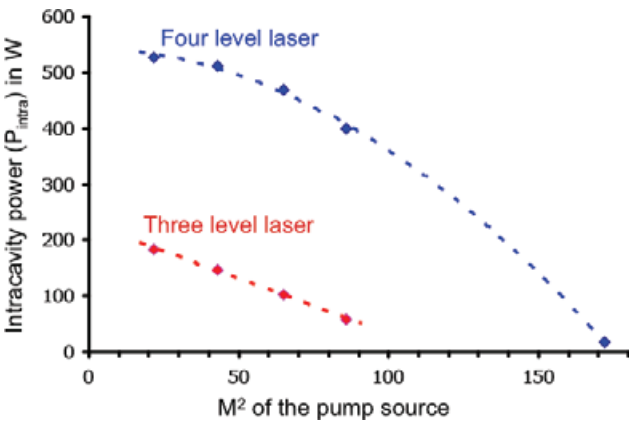

Figure 4 (online color at: www.lpr-journal.org) Evolution of the intracavity power P_{intra} versus the M^2 of the pump diode.

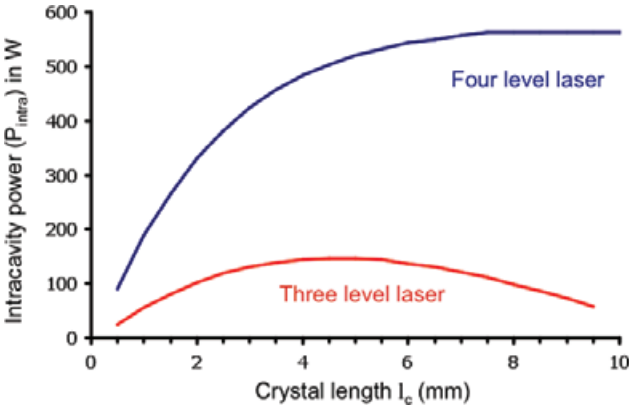

Figure 5 (online color at: www.lpr-journal.org) Evolution of the intracavity power P_{intra} versus the crystal length l_c.

laser shows that it is more tolerant to this parameter when M^2 remains below 70.

Another way to view the problems of reabsorption in a three-level laser is to investigate the effect of the crystal length l_c on the intracavity power. Figure 5 shows that there is an optimum: if the crystal is too short, the very small pump absorption limits the laser efficiency. On the other hand, a crystal too long leads to reabsorption at the laser wavelength because the pump transparency is not reached in the last millimeters. Consequently, the pump power can not be totally absorbed in the case of a three-level laser. As an example, the absorption is 50% in the case of the Nd:GVO_4 with an optimized length at 5 mm. This is another factor that reduces the efficiency compared to a four-level system where all the pump power can be absorbed. Note that a double-pass pumping scheme could be considered to avoid this problem. However, it is more complex to implement and the feedback in the laser diode may reduce its lifetime.

The next step of this theoretical study is to see the influence of the cavity losses on the intracavity power. Figure 6 shows that is it a key parameter for the laser design, a three-level laser being much more sensitive to losses that a four-level laser.

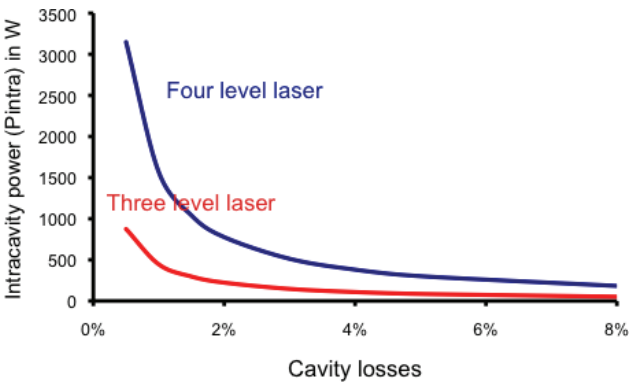

Figure 6 (online color at: www.lpr-journal.org) Evolution of the intracavity power P_{intra} versus the cavity losses.

3.3. Discussion on the guidelines

The previous results show that a bulk diode-pumped three-level laser needs to be designed very carefully. As for all lasers, the pump needs to be as bright as possible and the cavity losses as low as possible. However, compared to a four-level laser, the effects of those two parameters are more pronounced (particularly for the losses).

The signal beam size and the crystal length need to be optimized in order to avoid the reabsorption losses and the tolerance on those parameters is very low compared to a four-level laser. Moreover, the tolerance depends strongly on the laser design. Figure 7 shows that the optimal length is completely different following the doping concentration selected (0.1%, 0.2% or 0.3%). Moreover, the curve at 0.3% is more peaked (with a full width at half-maximum (FWHM) of 5 mm) than the one at 0.1% (with a FWHM of 8.4 mm). This is related to the lower absorption of the 0.1% doped crystal.

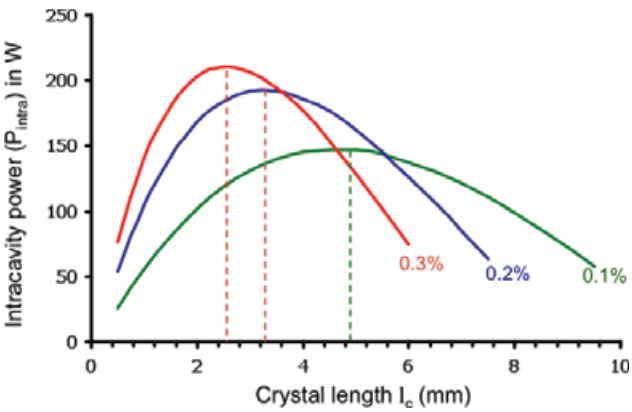

Figure 7 (online color at: www.lpr-journal.org) Evolution of the intracavity power P_{intra} versus the crystal length for three different doping concentrations in Nd:$GdVO_4$.

The pump polarization is also an important parameter for polarization-dependent crystals. For examples, the Nd:vanadate crystals can be oriented to benefit from the lowest pump transparency (pump polarization parallel to the π axis), as explained in Table 1. However, a fiber-coupled laser diode is often unpolarized. The pump transparency expression needs to be modified in order to take this effect into account. Assuming that the pump intensity is equally distributed on the two crystal axes σ and π, we can write the average pump transparency:

$$\overline{I_{\text{ptr}}^{\text{unpol}}} = \frac{hc}{\lambda_p} \frac{\sigma_{\text{al}}}{\left(\overline{\sigma_{\text{ap}}^{\sigma}} + \overline{\sigma_{\text{ap}}^{\pi}}\right) \cdot \sigma_{\text{el}}} \cdot \frac{1}{\tau}, \tag{16}$$

where $\overline{\sigma_{\text{ap}}^{\pi}}$ and $\overline{\sigma_{\text{ap}}^{\sigma}}$ are the average cross sections on the π-axis and on the σ-axis, respectively. In the case of Nd:$GdVO_4$, the unpolarized pump transparency is 16.7 kW/cm^2, to be compared with the 10.4 kW/cm^2 for a pump polarized on the π-axis.

The difference between those two values induces a dramatic effect on the intracavity power, as shown on Fig. 8.

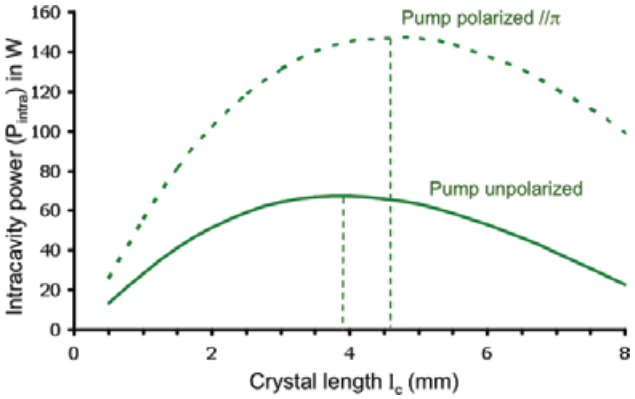

Figure 8 (online color at: www.lpr-journal.org) Evolution of the intracavity power P_{intra} versus the crystal length for an unpolarized pump beam and for a π-polarized pump beam.

The laser pumped by an unpolarized beam has an intracavity power reduced by a factor of 2.3. Moreover, the optimum crystal length is shifted towards lower values as a combined effect of the higher pump transparency and of the imperfect overlap between the pump beam and the cavity beam.

Finally, one has to mention the importance of the criteria chosen for the optimization. As a fundamental laser parameter, it is generally admitted that optimizing the small signal G_0 is a good way to optimize the laser efficiency. One can find an expression for G_0 using Eq. (15) and setting the signal to $I = 0$. However, in the case of a three-level laser, it is not that obvious. Figure 9 compares the curves P_{intra} and G_0 versus the crystal length. The G_0 curve appears clearly to be shifted towards higher values of crystal lengths. This effect is due to saturation of absorption at the beginning of the crystal. As the pump is less absorbed, a value of pump intensity higher than I_{ptr} can be maintained over a longer distance. The situation is different when we consider the intracavity power: as the laser is running, the signal intensity is significant and it reduces the population of the upper level. Consequently, the crystal absorption is higher and the optimum length is lower.

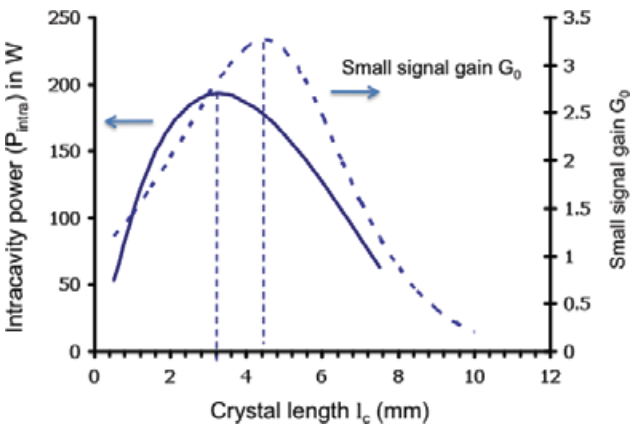

Figure 9 (online color at: www.lpr-journal.org) Comparison of intracavity power and small-signal gain curves versus the crystal length. The Nd doping concentration is 0.2%.

In this section, the effects of the different parameters were investigated assuming that the three-level laser line is the only one. However, the real case is more complicated, as Nd^{3+} ions generally have a lot of energy levels (see for example, the energy levels of Nd:YAG reported in Fig. 1). In order to operate Nd:lasers at low emission wavelengths, we also have to consider the line competition. The next section gives examples: Nd:YAG operating as a quasi-three-level laser with a lower level of the laser transition being highly populated and Nd:vanadates crystals operating as pure three-level lasers.

4. Low laser wavelength emission with Nd:YAG and Nd:vanadates

In order to demonstrate experimentally the possibility to operate below 900 nm with Nd-doped crystals, we have chosen Nd:YAG because it is the most known Nd:doped crystal. Moreover, Table 1 shows that the pump transparency is low for laser emission at 899 nm and 884 nm. The other crystals considered are vanadate crystal and mainly Nd:$GdVO_4$, which presents a very low pump transparency intensity for three-level laser operation at 879 nm. Here, we use the guidelines of the previous part: pumping short and low-doped crystals with high brightness laser diodes.

4.1. Nd:YAG laser emitting below 900 nm

As shown on Fig. 1, many laser transitions are possible for Nd:YAG. The lines differ on two quantities: the emission cross section and the absorption cross section. Figure 10 shows that the shorter the wavelength, the higher the absorption cross section. This is of course related to the thermal population, which is very different following the levels (as shown on Fig. 1). The well-known 946-nm transition presents nearly no absorption in comparison with the laser lines below 900 nm. On the other hand, the absorption is higher than the emission for the pure three-level laser line at 869 nm.

In order to understand the behavior of the different lines with the pump power, we calculate the small-signal gain G_0

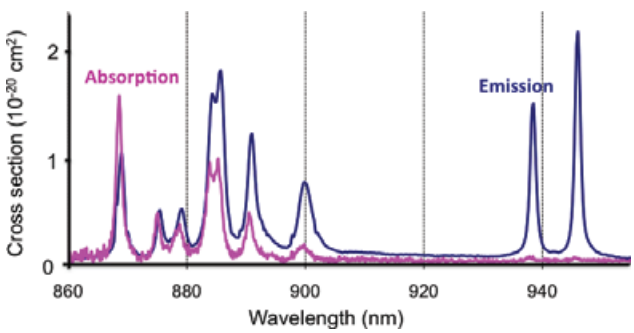

Figure 10 (online color at: www.lpr-journal.org) Emission and absorption cross section of Nd:YAG from [38].

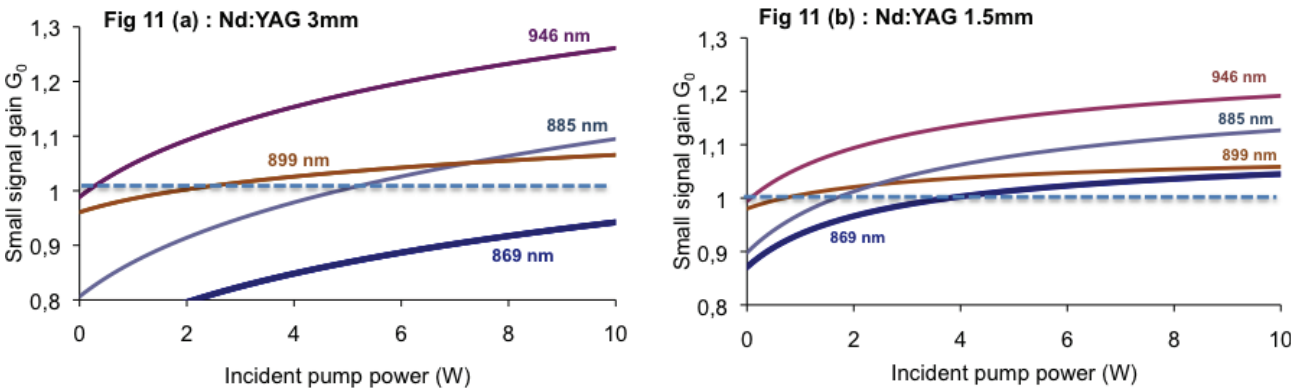

Figure 11 (online color at: www.lpr-journal.org) Small-signal gain G_0 for four Nd:YAG laser lines versus the pump power. The simulation parameters are: doping concentration = 0.5%, $w_{p0} = 50\,\mu m$, $M^2 = 43$, $w_0 = 40\,\mu m$. The crystal length is $l_c = 3\,mm$ for Fig. 11a and $l_c = 1.5\,mm$, for Fig. 11b.

for a few significant wavelengths of Nd:YAG below 950 nm: 869 nm, 885 nm, 900 nm and 946 nm. Figure 11a shows that the curves are completely different. The 946 nm starts with a gain very close to 1 (because the transparency intensity is very low) and overcomes the other lines because the emission cross section is the highest in this wavelength range. The 899 nm reaches a small-signal gain of 1 at a moderate pump level. It is overcome by the 885-nm laser line above 7 W of incident pump power because the emission cross section is higher at 885 nm than at 899 nm. The 869 nm line remains with a gain < 1 meaning that laser oscillation is impossible for this pump power range and for this crystal length.

As shown in Sect. 3, the crystal length is a key parameter for laser operation in a three-level system. We investigate its influence by computing the small-signal gain on the different lines for a shorter Nd:YAG crystal (1.5 mm). The results are given in Fig. 11b). The gain at 946 nm is lower in comparison to Fig. 11a because the number of excited atoms is lower. However, the gain is higher for the 885 nm transition because there is no reabsorption at the end of the crystal. At 869 nm, the gain is now higher than 1, showing that laser action on this pure three-level laser line is possible. Therefore, the choice of the crystal length can be seen as a first way to select the wavelength: a long crystal will promote laser lines with small absorption cross sections. Very short crystals are necessary to achieve laser amplification in the lines that are closer to the three-level system.

The first Nd:YAG laser cavity designed for the study of laser emission below 900 nm is described on Fig. 12. The crystal used is a 3-mm long 0.5%-doped Nd:YAG. As predicted by Fig. 11a, it should be short enough to demonstrate laser operation at 899 nm or even at 885 nm. The laser is pumped by a fiber-coupled laser diode emitting 10 W at 808 nm in a fiber core of 100 µm with a numerical aperture of 0.22. The output of the fiber is imaged in the Nd:YAG by two doublets of 60 mm focal length. The cavity consists of 3 mirrors. M_1 is a dichroïc mirror with high transmission at 808 nm and high reflection between 850 nm and 950 nm. M_2 is a concave mirror with a radius of curvature of 200 mm. It is also highly reflective between 850 nm and 950 nm. In addition, it has a high transmission at 1064 nm in order to avoid laser emission on this strong gain four-level transition. M_3 is the output coupler. Its transmission is 2.8% at 899 nm.

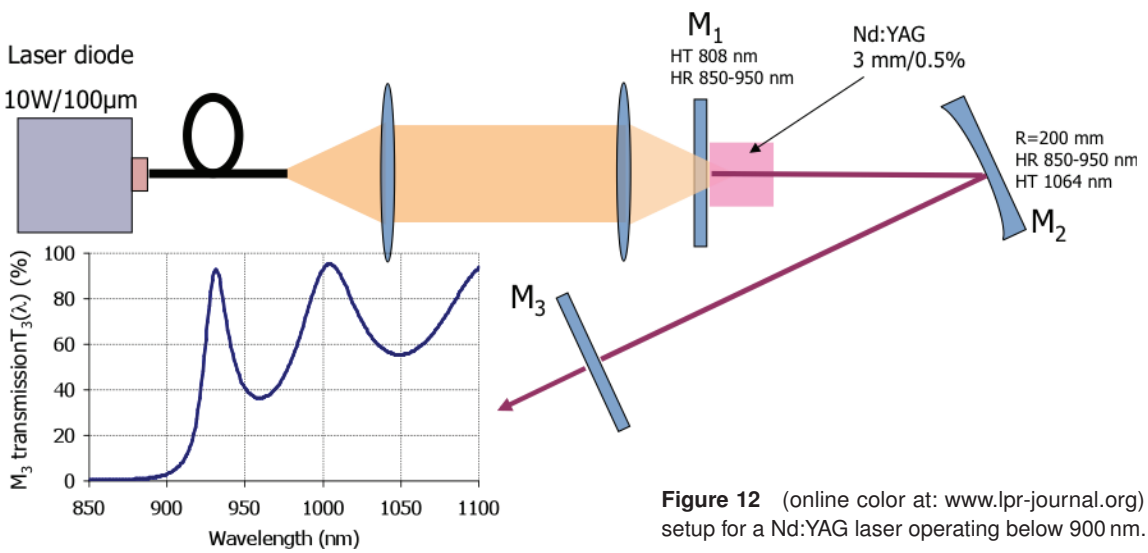

Figure 12 (online color at: www.lpr-journal.org) Experimental setup for a Nd:YAG laser operating below 900 nm.

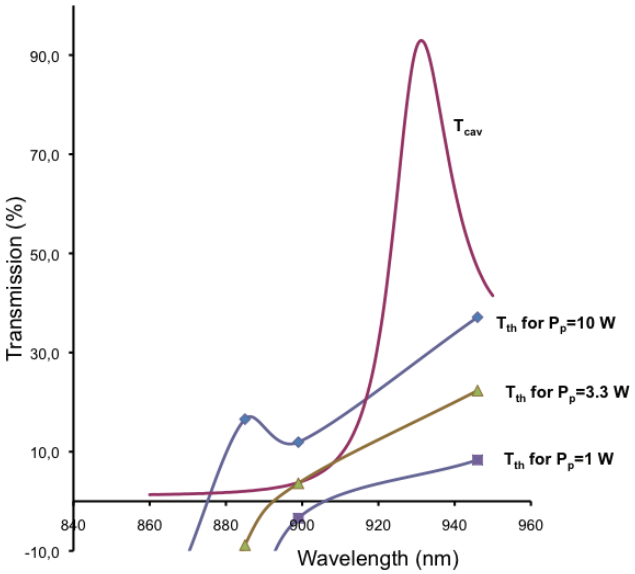

Figure 13 (online color at: www.lpr-journal.org) Comparison of the threshold cavity transmission T_{th} with the cavity transmission T_{cav} for different pump powers. T_{th} is calculated at 869 nm, 885 nm, 899 nm and 946 nm for Nd:YAG. The line between the points is only for clarity. The value for 869 nm is so negative that it is not represented on the graph.

Its spectral curve transmission $T_3(\lambda)$ is also given in Fig. 12: the shape is chosen to avoid laser emission at 946 nm.

In order to understand the line competition under laser operation, we define T_{cav} the transmission of the "cold" cavity (i.e. without the gain media) after one roundtrip. As the mirror transmission depends on the wavelength, T_{cav} is a function of λ. This quantity results from the knowledge of the transmission curves of the cavity mirrors and the knowledge of the passive losses L (supposed to be independent of the wavelength). Consequently:

$$T_{cav}(\lambda) = 1 - (1 - T_1(\lambda)) \cdot (1 - T_2(\lambda)) \cdot (1 - T_3(\lambda)) \cdot (1 - L) , \quad (17)$$

where $T_1(\lambda)$, $T_2(\lambda)$, and $T_3(\lambda)$ are the transmissions of the mirrors M_1, M_2, M_3, respectively.

At a fixed incident pump power P_p, we define the threshold cavity transmission $T_{th}(\lambda, P_p)$ corresponding to the value of the cavity transmission needed to reach the oscillation threshold at the considered wavelength. Following this definition, T_{th} is related to the small-signal gain by:

$$T_{th}(\lambda, P_p) = 1 - \frac{1}{G_0^2(\lambda, P_p)} . \quad (18)$$

The interest of T_{th} is that the study on the line competition can be concentrated on the transmission of the mirrors: if $T_{th} < T_{cav}$, laser oscillation is possible. If $T_{th} > T_{cav}$, the pump power is not high enough to reach the threshold.

Figure 13 presents the threshold cavity transmission T_{th} that is calculated at 869 nm, 885 nm, 899 nm and 946 nm for three pump powers. The line between the points is only for the legibility of the graph. A value of zero for T_{th} means that the laser must operate without losses to reach the oscillation threshold: this value is obtained when the pump power is equal to the pump transparency (i.e. G_0 is equal to unity). A negative value for T_{th} would correspond to an absorbant laser medium, the population inversion being not high enough to reach the transparency (i.e. G_0 is less than unity). It has no physical significance: it just indicates that the oscillation threshold can not be reached. The value for 869 nm is so negative that it is not represented on the graph. From Fig. 13, we can deduce that the oscillation threshold can never be reached at 946 nm, thanks to the coating on M_3. The curve for $P_p = 10$ W shows that laser oscillation could be reach for 885 nm and 899 nm. However, one has to know which wavelength reaches the threshold first. The curve for $P_p = 3.3$ W shows that the 899 nm is the first one. Once the laser oscillates at 899 nm, the gain is clamped at the values obtained for $P_p = 3.3$ W. This means that the oscillation threshold is never reached at 885 nm.

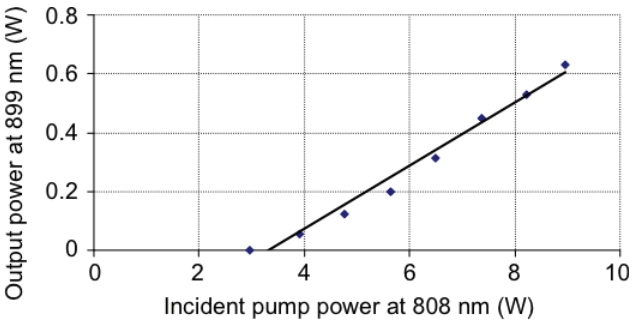

Figure 14 (online color at: www.lpr-journal.org) Laser output power at 899 nm versus the pump power for Nd:YAG from [38].

Indeed, this laser behavior is experimentally observed: with the setup presented on Fig. 12, laser oscillation is only achieved at 899 nm. The slope efficiency curve is presented in Fig. 14. Note that the simulations are consistent with the laser threshold found experimentally at 899 nm (around 3 W of incident pump power) with passive losses estimated at 1%.

The wavelength selection can also be achieved by the insertion of a spectrally selective element in the cavity. As an example, with a 25-μm thick Fabry–Perot etalon, we are able to select laser emission at 884 nm (16 mW of output power), at 891 nm (100 mW) or 899 nm (325 mW) [38]. However, the output power is reduced by a factor of two at 899 nm because of the additional losses introduced by the etalon. Therefore, we preferred to carry on our study with a spectral selection using mirror transmissions and crystal length, without any additional lossy element in the cavity.

In order to achieve laser emission at 885 nm, we chose a shorter crystal (2 mm long 0.5% doped), a higher power laser diode (emitting up to 25 W at 808 nm on a fiber core of 100 μm diameter) and a mirror M_3 having a larger transmission at 899 nm. The transmission cavity is reported in Fig. 15 (transmission curve denoted T_{cav} for 885 nm). This time, laser oscillation can not be reached at 899 nm and the first wavelength to reach the threshold is 885 nm for a

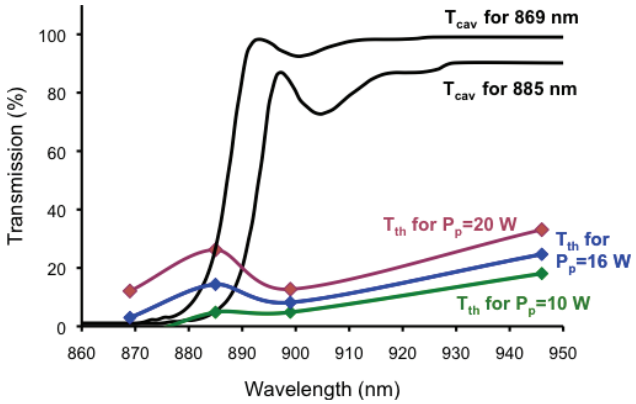

Figure 15 (online color at: www.lpr-journal.org) Cavity transmission in two-laser configuration (see the text). The threshold cavity transmission T_{th} is calculated for 869 nm, 885 nm, 899 nm and 946 nm for three pump powers.

pump power of 10 W. This is observed experimentally. We obtained a maximum power of 225 mW at 885 nm for a incident pump power of 20 W (Fig. 16). The oscillation at 869 nm was not observed in this configuration (even if $T_{th} < T_{cav}$) because the 885 nm line reaches the threshold first.

Figure 15 shows the possibility to obtain laser oscillation at 869 nm providing that the threshold is reached first on this wavelength. For that, we modified the setup as described on Fig. 17. The spectrally selective mirror M_3 is now used as a folding mirror. Hence, the laser beam passes two times per roundtrip on M_3, increasing the losses at 885 nm. Moreover, as the mirror is used with an incident angle of 10°, the transmission curve is blue shifted by approximately 4 nm. This effect increases also the losses at 869 nm. This new setup leads to the transmission cavity presented on Fig. 15 (T_{cav} for 869 nm). This time, the first wavelength reaching the laser threshold is 869 nm. This was experimentally observed and we obtained an output power of 8 mW with a laser threshold at 16 W of incident pump power.

With a higher pump power (40 W), Lü et al [46] demonstrated a laser emitting 453 mW at 869 nm. Key points for this experiment are the coating of the output mirror, the pump power and also a control of the cavity mode through a lithium niobate adjustable lens. As reported in Sect. 3, the overlap between pump and signal beams plays an important role in the efficiency of a three-level laser.

Even if it has been observed, the laser efficiency obtained with Nd:YAG on the pure three level transition at 869 nm is very low. As shown in Table 1, Nd:YAG is not the best choice for three-level laser operation. Nd vanadate crystals have cross sections one order of magnitude higher. Even if the pump transparency intensity is similar between Nd:YAG and Nd:YVO_4, it is three times lower for Nd:$GdVO_4$ (due to the singular increase in the pump absorption cross section). In the next part, we investigate the potential of those Nd-doped vanadate crystals as three-level lasers.

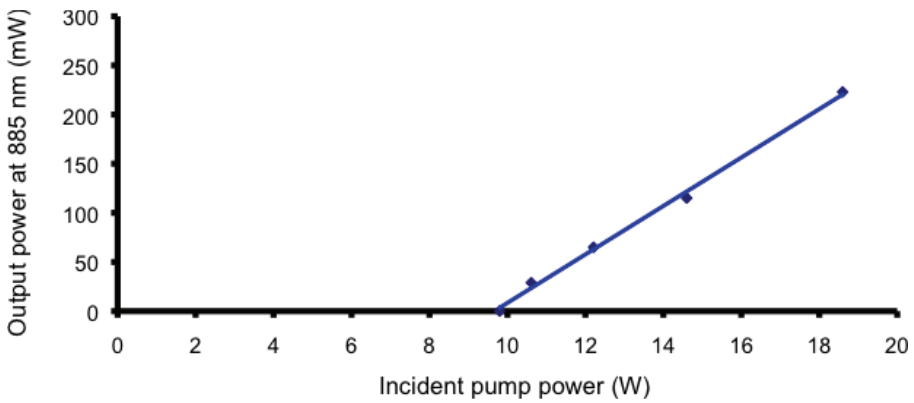

Figure 16 (online color at: www.lpr-journal.org) Laser output power at 885 nm versus incident pump power.

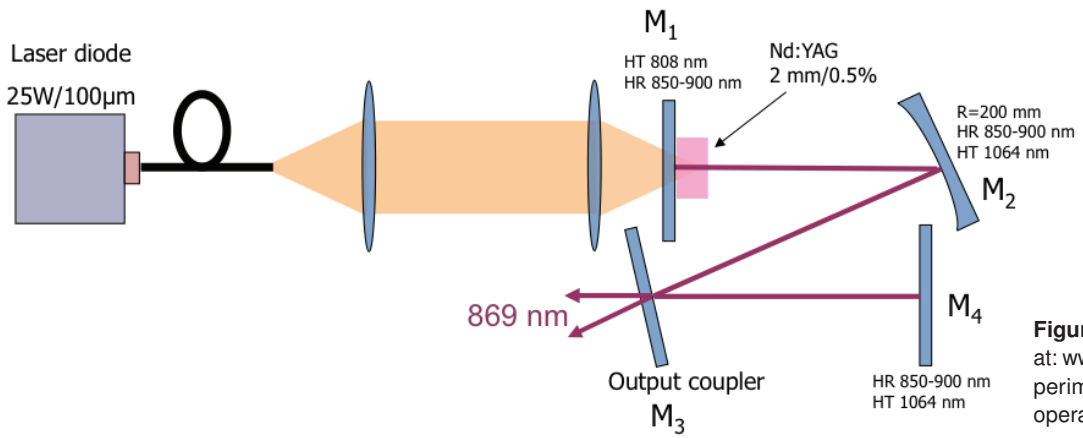

Figure 17 (online color at: www.lpr-journal.org) Experimental setup for laser operation at 869 nm.

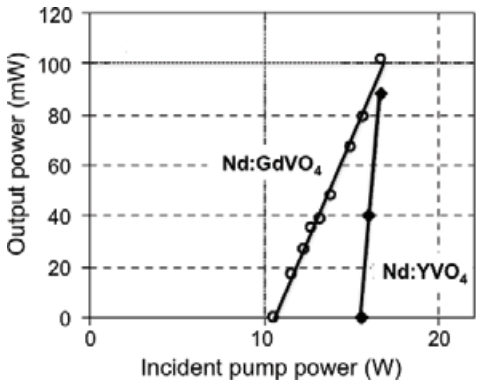

Figure 18 Comparison of laser emission around 880 nm versus the pump power for Nd:YVO_4 and Nd:$GdVO_4$ from [47].

4.2. Nd:vanadates as pure three-level lasers

The first experiment carried out is a comparison between Nd:YVO_4 and Nd:$GdVO_4$ for laser emission at 880 nm and 879 nm, respectively. For that, we use a cavity relatively similar to that of Fig. 12. This time, the laser diode is a fiber coupled 20 W system with a core fiber of 200 µm (NA = 0.22) with a M^2 factor of 80. The vanadate crystals are 0.2%-doped 4-mm long samples. The spectral selectivity is achieved with a 25-µm etalon. The output coupler has a transmission of 3% at 880 nm. M_1 and M_2 are the same as in Fig. 12. Figure 18 shows the output powers obtained. We observe that the oscillation threshold is higher for Nd:YVO_4. This can be related to the higher pump transparency intensity. Moreover, below the threshold, we observe a laser emission at 1064 nm occurring between the crystal faces. This is not the case with Nd:$GdVO_4$ whose emission cross section peaking at 1063 nm, is lower. Hence, we find that Nd:$GdVO_4$ is easier to use for the three-level laser operation. So, Nd:$GdVO_4$ crystal is used for the following experiments described in this section.

The next experiment is designed in order to optimize the output power at 879 nm with Nd:$GdVO_4$. Once again, the setup used is basically the same as the one described in Fig. 12. Following Sect. 3, the pump laser diode is replaced by a brighter laser diode (25 W 100 µm core fiber, NA = 0.22). The Nd:$GdVO_4$ is a 5-mm long 0.1%-doped sample with faces antireflection coated between 800 and 1100 nm.

In Nd:$GdVO_4$, only two main laser lines appear on the π polarization: the emission at 879 nm and the emission at 912 nm. In order to manage the line competition we propose here a different way from the one presented for Nd:YAG. It is based on the values of the emission cross section: higher at 879 nm than at 912 nm. Therefore, once the pump transparency is reached at 879 nm, the gain becomes rapidly higher at this wavelength. This effect is clearly visible in Fig. 19 showing the threshold cavity transmission for the two wavelengths versus the pump power. The mirror M_3 is chosen with a high transmission (25%) but flat with respect to the wavelength in the 850–950 nm range. The transmission cavity is therefore independent of the wavelength and it can be represented in Fig. 19 by a horizontal line (transmission of 28%, including the passive losses). Figure 19 shows that the first wavelength reaching the oscillation threshold is 879 nm, when the pump power is increased. Thus, the oscillation at 912 nm is never reached due to lines competition.

Figure 20 gives the output power versus the incident pump power. We demonstrate a maximum of 2 W at 879 nm. Close to the threshold, we observe parasitic laser oscillation at 1064 nm between the two faces of the Nd:$GdVO_4$ crystal. This effect disappears at 17 W of incident pump power. This effect reduces the population in the upper level and shifts the threshold towards higher values. The inset of Fig. 20 shows the beam profile, which is close to a gaussian one, with a M^2 value measured at 1.5.

The wavelength selection by the gain can be used with transmission higher than 22% corresponding to the intersection of the two threshold cavity transmissions T_{th} at 912 nm and at 879 nm (Fig. 19). Below this value, one has to use a spectral selective mirror as M_3 as in Nd:YAG. Figure 21shows the output power versus the transmission of the output coupler. The three lowest transmissions are achieved

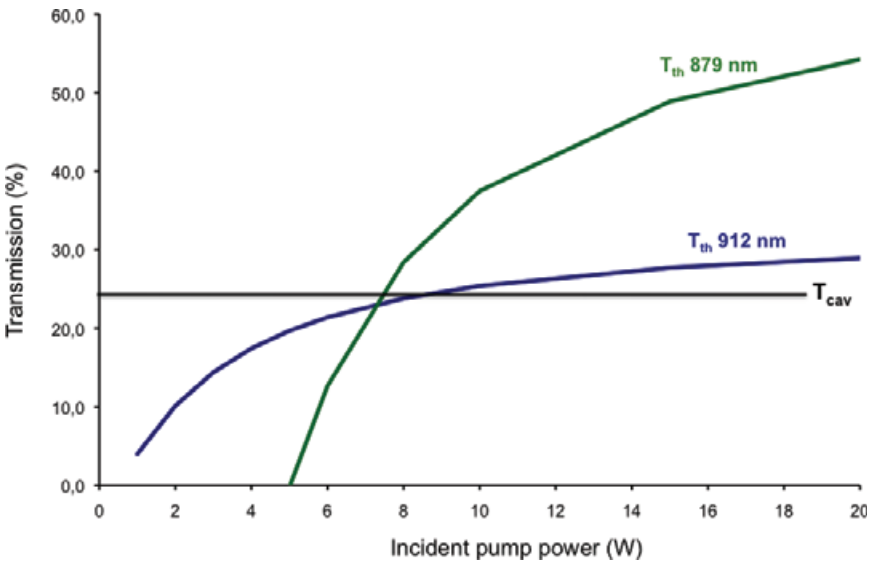

Figure 19 (online color at: www.lpr-journal.org) Comparison of the threshold cavity transmission for 912 nm and 879 nm versus the pump power. The transmission cavity is also represented on this graph.

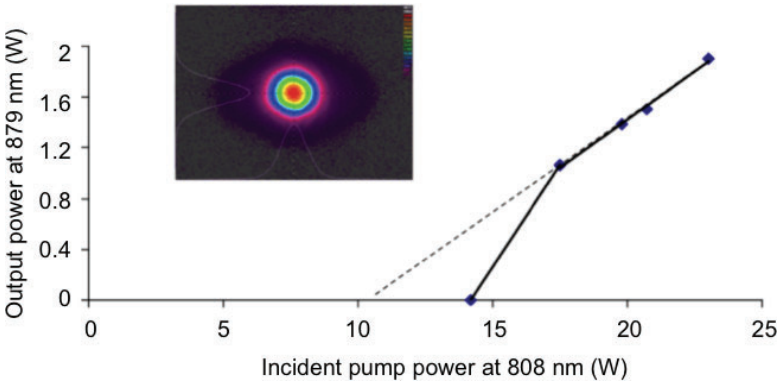

Figure 20 (online color at: www.lpr-journal.org) Output power versus pump power for Nd:$GdVO_4$ laser operation at 879 nm. Inset: spatial beam profile from [48].

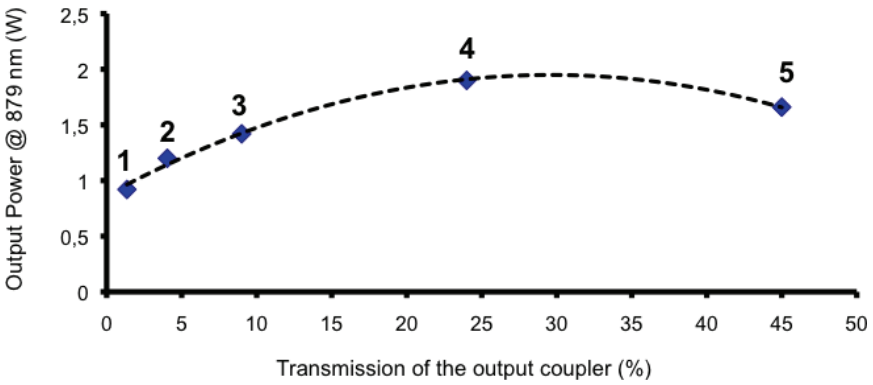

Figure 21 (online color at: www.lpr-journal.org) Output power versus the transmission of the output coupler of the Nd:$GdVO_4$ laser operating at 879 nm. The points 1, 2 and 3 are obtained with spectrally selective mirrors. The points 4 and 5 are obtained with flat transmission output couplers.

with wavelength-selective mirrors. The two highest transmissions are achieved with output couplers having a flat transmission versus the wavelength. This curve shows that the optimum is close to the transmission of 25% corresponding to the results presented in Fig. 20.

For the lowest transmission (1%) the intracavity power reaches 68 W. Even if it is lower than the intracavity power generally produces at other wavelengths (such as 912 nm or 1064 nm), this level is enough to try second-harmonic generation by the insertion of a nonlinear crystal in the cavity. This is the purpose of the next section.

5. Emission below 450 nm by intracavity second-harmonic generation

In this section we investigate second-harmonic generation based on the previous studies. We take two examples: Nd:YAG with generation at 449.5 nm and Nd:$GdVO_4$ with generation at 439.5 nm.

Note that extracavity second-harmonic generation can be achieved simply by focusing the output of the laser in a nonlinear crystal. However, in order to achieve high conversion efficiency, specific nonlinear crystals are required: periodically poled lithium niobate for example or waveguides in order to confine the fundamental beam [3]. In our case, we design a laser using conventional nonlinear crystals: this requires putting the nonlinear crystal inside the cavity, where the intensity is much higher. The laser cavity needs to be redesigned for this purpose. Moreover, one has also to take the line competition in account.

The laser cavity for the Nd:YAG is shown in Fig. 22. The pump laser diode and the Nd:YAG crystal are the same as the one presented on Fig. 12. In order to avoid laser oscillation at 946 nm (and 1064 nm) while having high intracavity power at 899 nm, we chose a high-reflectivity coating from 800 nm to 900 nm for the mirrors M_2 and M_3. As the 899-nm laser line will always reach laser oscillation before the 885 nm and the 869 nm line (Fig. 13), the mirror coating does not have to be spectrally selective for lines below 899 nm.

M_2 and M_3 are concave mirrors in order to create a small waist (radius 20 µm) within the nonlinear crystal. The passive losses are estimated to 3% and the intracavity power at 25 W. The nonlinear crystal used is a 10 mm long LBO ($\theta = 90°$, $\varphi = 22.86°$).

Figure 23 gives the output power in the blue (after the sum of the two outputs through M_2 and M_3). A maximum power of 100 mW is obtained for an incident pump power of 9 W.

After this first demonstration, the design has been improved by another research team [49]: the pump power is doubled and the nonlinear crystal used is a BiBO. Indeed, Table 2 shows that the nonlinear properties of BiBO are better than LBO for the second-harmonic generation at 449.5 nm. Note that the potassium niobate has a higher nonlinear coefficient but that the walk-off is very large. The experimental setup is very close to the one presented in Fig. 22. An output power of 300 mW has been obtained at 449.5 nm.

Emission at 439.5 nm is carried out with Nd:$GdVO_4$. In order to increase the nonlinear conversion, we decide to use a $KNbO_3$ crystal in the noncritical phase matching configuration. Indeed, Table 3 shows that the nonlinear properties of $KNbO_3$ are very interesting in comparison to LBO and

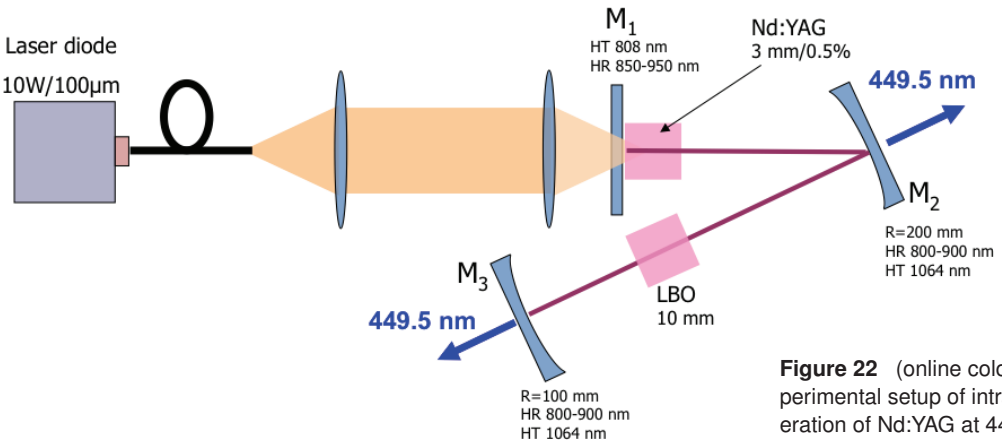

Figure 22 (online color at: www.lpr-journal.org) Experimental setup of intracavity second-harmonic generation of Nd:YAG at 449.5 nm.

Table 2 Properties of different nonlinear crystals for second-harmonic generation in the blue (899 nm → 449.5 nm).

Crystal	Orientation	D_{eff} (pm/V)	Walk-off (mrad)	Thermal acceptance (K cm)	Angular acceptance (mrad cm)	Spectral acceptance (nm cm)
LBO (300 K)	$\theta = 90°$ $\varphi = 22.86°$	0.80	13	7.7	4.3	38.5
BiBO (300 K)	$\theta = 158.6°$ $\varphi = 90°$	3.48	47	1.9	1.1	11.2
$KNbO_3$ (300 K)	$\theta = 90°$ $\varphi = 69°$	12.8	36.5	0.4	1.1	3.1

Table 3 Properties of classical nonlinear crystals for second-harmonic generation in the blue (879 nm → 439.5 nm).

Crystal	Orientation	D_{eff} (pm/V)	Walk-off (mrad)	Thermal acceptance (K cm)	Angular acceptance (mrad cm)	Spectral acceptance (nm cm)
LBO (300 K)	$\theta = 90°$ $\varphi = 24.4°$	0.79	3.99	8.04	3.99	2.7
BiBO (300 K)	$\theta = 157.4°$ $\varphi = 90°$	3.53	0.99	1.77	0.99	0.81
$KNbO_3$ (369 K)	Noncritical phase matching	13.7	0	0.30	Infinity at first order	0.22

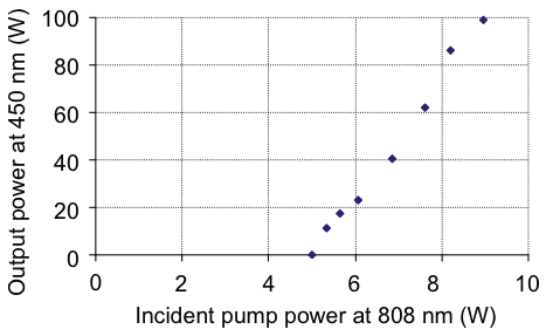

Figure 23 (online color at: www.lpr-journal.org) Output power (sum of the two outputs) at 449.5 nm for the laser presented on the Fig. 22 from [38].

even to BiBO. The nonlinear coefficient is very high and the noncritical phase matching configuration allows focusing of the fundamental beam tightly in order to increase the nonlinear efficiency. However, the crystal has to be maintained at a fixed temperature (369 K) and the spectral acceptance is very low: only 0.22 nm for the 10-mm long crystal used in this experiment.

The laser setup is given in Fig. 24. This time, we use a four-mirror cavity. The reason for this is that the wavelength selection needs to be done by mirrors transmission in a low-loss cavity. We used two mirrors (M_3 and M_4) having high transmission beyond 900 nm. This leads to the cavity transmission shape given in Fig. 25. The value of transmission is enough to avoid laser oscillation at 912 nm (as shown by the

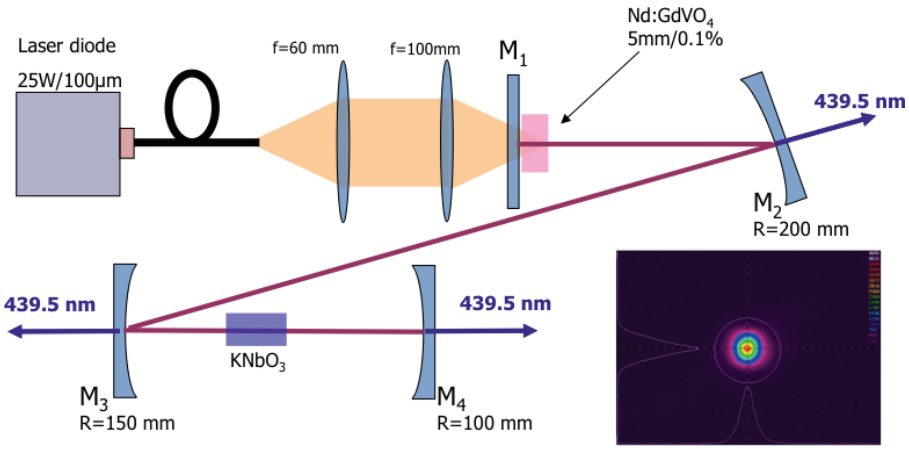

Figure 24 (online color at: www.lpr-journal.org) Experimental setup for the Nd:$GdVO_4$ laser emitting at 439.5 nm by second-harmonic generation. Inset: output beam profile at 439.5 nm.

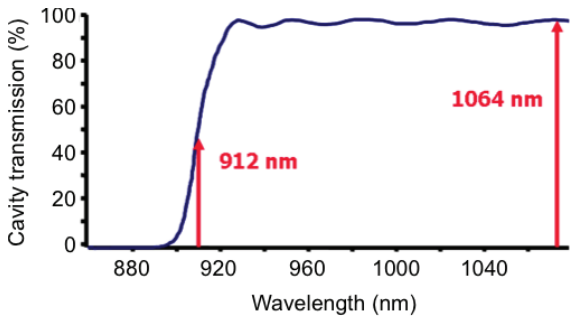

Figure 25 (online color at: www.lpr-journal.org) Shape of the cavity transmission described in Fig. 24.

maximum T_{th} value at 912 nm given in Fig. 19). The potassium niobate crystal is placed at the focus point between M_3 and M_4.

In this cavity we observe three significant outputs in the blue (through M_2, M_3 and M_4). At maximum pump power, the sum of the three ouputs equals 300 mW at 439.5 nm. The M^2 is measured below 1.5. Figure 26 is an enlargement of the nonlinear crystal.

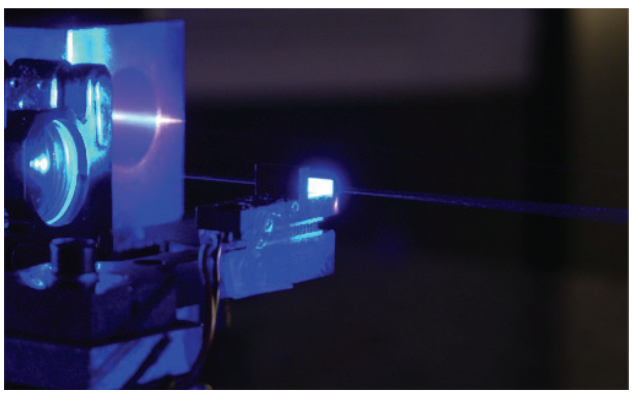

Figure 26 (online color at: www.lpr-journal.org) Photo of the potassium niobate crystal under laser operation. The thermoelectric cooler used for the temperature regulation is clearly visible below the crystal mount.

6. Discussion and conclusion

This paper presents the specificities of diode-pumped neodymium lasers operating below 900 nm, either on a three-level system or on a quasi-three-level system having its lower level close to the ground state. It also explains how to manage the competition with the other lines, mainly at higher wavelengths. The paper presents the lasers developed and the performance obtained in Nd:YAG and Nd-doped vanadates. The overall laser efficiency in the infrared (i.e. the output power over the incident pump power) is between 1% and 10% following the wavelength and the gain medium. Compared to the efficiency generally obtained with the same crystals at 1064 nm or even at 946 nm (Nd:YAG) or at 914 nm (Nd:YVO_4), these values are very low. This is a consequence of the three-level nature of the transitions. Sect. 2 explains that the key parameter is the pump transparency intensity. In a simple approximation, the efficiency of the laser can be given by:

$$\eta = \frac{\lambda_p}{\lambda}\Gamma\frac{I_{pinc} - I_{ptr}}{I_{pinc}} \tag{19}$$

where Γ is a coefficient related to the overlap between the pump and the signal and I_{pinc} is the pump intensity incident on the crystal. Equation (19) shows that the pump intensity needs to be very high in comparison to I_{ptr} in order to reach a good efficiency and to tend towards the ultimate quantum efficiency. This can be achieved in fibers where the beam confinement is realized via the guiding of pump and signal beams. As an example, efficient three-level laser operation has already been demonstrated at 980 nm [7, 8]. In the case of bulk crystals, it is more complicated to have a good efficiency because the beams are in free-space propagation. Roughly speaking, the pump intensity is high only close to the focus. The reabsorption losses can appear at many places: on the beam edges, out from the focus point and at the end of the crystal in the case of a one-side longitudinal pumping. Sect. 3 explains these effects by showing the influence of the pump M^2, of the beam size, and of the crystal length on the laser power. This leads to a low absorption typically below 50% in order to maintain a pump intensity high enough at the end of the crystal.

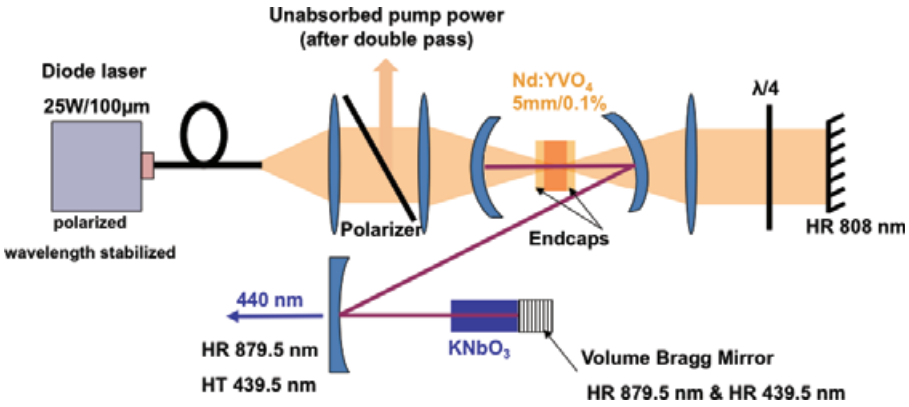

Figure 27 (online color at: www.lpr-journal.org) Proposed experimental setup for optimized laser operation at 439.5 nm with Nd:$GdVO_4$.

Even if it is intrinsically limited, it is possible to propose a setup optimizing the laser efficiency of the Nd-doped lasers emitting below 900 nm, following the theoretical studies and the experimental results presented in this paper. Figure27 gives an example in the case of Nd:$GdVO_4$ operating at 439.5 nm. First, one has to take care about the choice of the laser diode. It has to be as bright as possible (meaning the highest output power with the lowest M^2). The diode spectrum has to be reduced below 1 nm in order to take benefit of the peak absorption cross section and hence to reduce the pump transparency intensity. In the case of polarized crystals such that Nd:$GdVO_4$, the pump needs to be polarized in order to reduce the pump transparency intensity (Fig. 8 shows the dramatic effect of an unpolarized pump). One way to avoid reabsorption losses at the end of the crystal while improving the overall absorption is to recycle the pump beam. However, the feedback in the laser diode can have a deleterious effect on its lifetime. Following its beam-shaping system and the length of its output fiber, a pump laser diode system can have a polarized output. In this case, one possibility is to rotate the polarization with a quaterwave plate and to separate the pump beam after two passes from the incident beam by a polarizer (see Fig. 27). The temperature increase induced by the pump can also have problematic effects: the transverse temperature gradient in the crystal may induce a thermal lens and may also affect the beam quality. Moreover, the temperature increase is always related to a decrease of the cross sections [50] with an effect on the pump transparency intensity and on the laser efficiency. One way to reduce the temperature increase is to use a composite rod with a doped section sandwiched between two undoped endcaps. Another way could be to use a lower-doped crystal but one has to be careful with the overlap between the pump and the cavity beams. Next, the cavity has to ensure laser oscillation at the right wavelength. Section 4 shows that the dielectric coating of the mirrors needs to be chosen carefully in order to avoid the line competition. Another solution is to use a Bragg mirror with a reflectivity peaking at the considered wavelength. Finally, one has to select an efficient nonlinear crystal in order to achieve a good frequency conversion in the blue, since the intracavity power in a three-level laser is limited (as shown in the figures in Sect. 3). Only one output in the blue can be achieved if the Bragg mirror has two sections: one highly reflective at the fundamental wavelength and the other one highly reflective for the second harmonic. A more compact system could be also a microchip laser in which all the optical pieces are contacted together.

Table 4 Properties of diode-pumped solid-state laser sources emitting in the range 400–450 nm. SHG means second-harmonic generation. THG means third-harmonic generation by two nonlinear conversions stages. In the bottom of the table is the performance of blue laser diodes and helium-cadmium lasers. For all sources, only continuous wave operation with single transverse mode is considered.

Type of laser source	Wavelength	Output power
Nd:YAG 1319 nm + ppKTP (THG) [27]	440 nm	3.1 mW
Cr:LiSAF + $KNbO_3$ (SHG) [20]	427 nm	13 mW
Nd:YAG + BiBO (SHG) [46]	434.5 nm	118 mW
Nd:YAG + BiBO (SHG) [49]	449.5 nm	300 mW
Nd:$GdVO_4$ + $KNbO_3$ (SHG) [48]	439.5 nm	300 mW
Laser diode [51]	405 nm	120 mW
Laser diode [51]	440 nm	50 mW
Helium-cadmium [52]	442 nm	180 mW

In the blue, the Nd-doped laser source presented in this paper has an overall optical efficiency between 0.3% and 1.5% and a wall plug efficiency between 0.1% and 0.3%. This has to be compared with the efficiency of helium-cadmium lasers, typically below 0.03%.

Table 4 gives an overview of the performance obtained with diode-pumped solid-state lasers in the range 400–450 nm. For the comparison, we consider only lasers sources with $M^2 < 1.5$ since the beam quality is an important parameter for many applications in the blue. Apart from the Nd-doped lasers operating at low wavelengths, only two solutions are reported in the literature: Frequency-doubled Cr:LiSAF and frequency-tripled Nd:YAG. The output power is limited in both cases either by thermal problems or by inefficient nonlinear conversion. The Nd-doped lasers presented in this paper provide output powers more than one order of magnitude higher.

The performances obtained with Nd-doped lasers are higher than the output powers offered by commercial blue laser diodes and helium-cadmium lasers. Moreover, compared to laser diodes, low-wavelength Nd-doped lasers can

provide temporal coherence with a higher wall plug efficiency and higher lifetime than gas lasers. It is also worth noting that they require only commercially available elements that can be provided by many different companies. Hence, low-wavelength emission Nd-doped laser are very promising for applications in the blue range, namely below 450 nm.

Acknowledgements. Marc Castaing's Ph. D. was funded by OXXIUS.

Received: 21 December 2010, **Revised:** 7 February 2011, **Accepted:** 9 March 2011

Published online: 31 March 2011

Key words: Diode-pumped solid-state lasers, neodymium-doped lasers, three-level lasers, quasi-three-level lasers, blue lasers, second-harmonic generation.

François Balembois received an engineering degree in optics from Institut d'Optique in 1991 and the Ph. D. degree in physics from University Paris XI in 1994 for a dissertation on diode-pumped Cr:LiSAF lasers. He was an assistant professor from 1994 to 2003 and he is now a professor at the Institut d'Optique, since 2003. His research area concerns the development of new diode-pumped solid-state lasers covering the visible and the near-infrared including new crystals and new architectures. He studies pulsed lasers in different time regimes: from the nanosecond to the femtosecond regime.

Marc Castaing received an engineering degree in optics, from Institut d'Optique graduate school in 2006, and the M. S. in optics and photonics from Paris XI University in the same year. After three years of collaborative research between l'Institut d'Optique and Oxxius (a laser company based in Lannion, France) he obtained the Ph. D. degree in physics from Paris XI University in 2009, for a dissertation on three-level lasers in neodymium- and ytterbium-doped crystals. He is currently working as a research and development engineer at Lumera laser GmbH (Kaiserslautern, Germany) on new concepts for high-power picosecond systems.

Emilie Hérault received an engineering degree in optics, laser and plasma from Polytech'Orleans in 2002, the M. S. in optics and photonics from Paris XI University in 2003 and the Ph. D. degree in laser and nonlinear optics from Paris XI University in 2007, for a dissertation on new concepts for blue-laser sources based on neodymium-doped crystals. Since 2009, she has been an assistant professor in THz spectroscopy at the IMEP-LAHC laboratory, University of Savoie, where her activities are related to THz signal generation and detection and material characterization.

Patrick Georges received an engineering degree in optics from the Institut d'Optique, in 1985, and the Ph. D. degree in physics in 1989. He is currently a senior scientist at the CNRS and leads the Lasers and Biophotonics Group of the Laboratoire Charles Fabry de l'Institut d'Optique, Palaiseau. His current research concern: diode-pumped solid-state lasers, new rare-earth-doped laser materials for fs lasers, high-brightness laser diodes improvement, LMA fiber amplifier systems, new geometries of single-crystal fibers, wavefront control techniques in multimode or multicore fibers and optically pumped semiconductor lasers. He is also engaged in new high resolution imaging techniques such as optical coherence tomography, total internal reflexion imaging, two-photon absorption fluorescence lifetime or stimulated emission depletion microscopies for biophotonics applications.

References

[1] S. Nakamura, S. Pearton, and G. Fasol, The Blue Laser Diode: The Complete Story (Springer, Berlin, Heidelberg, 2000).
[2] C. Fiebig, A. Sahm, M. Uebernickel, G. Blume, B. Eppich, K. Paschke, and G. Erbert, Opt. Express **17**, 22785–22790 (2009).
[3] A. Jechow, M. Schedel, S. Stry, J. Sacher, and R. Menzel, Opt. Lett. **32**, 3035–3037 (2007).
[4] T. Y. Fan and R. L. Byer, Opt. Lett. **12**, 809–811 (1987).
[5] C. Czeranowsky, E. Heumann, and G. Huber, Opt. Lett. **28**, 432–434 (2003).
[6] Q. H. Xue, Q. Zheng, Y. K. Bu, F. Q. Jia, and L. S. Qian, Opt. Lett. **31**, 1070–1072 (2006).
[7] J. Boullet, Y. Zaouter, R. Desmarchelier, M. Cazaux, F. Salin, J. Saby, R. Bello-Doua, and E. Cormier, Opt. Express **16**, 17891–17902 (2008).
[8] F. Röser, C. Jauregui, J. Limpert, and A. Tünnermann, Opt. Express **16**, 17310–17318 (2008).
[9] D. B. S. Soh, C. Codemard, S. Wang, J. Nilsson, J. K. Sahu, F. Laurell, V. Philippov, Y. Jeong, C. Alegria, and S. Baek, IEEE Photon. Technol. Lett. **16**, 1032–1034 (2004).
[10] A. Bouchier, G. Lucas-Leclin, and P. Georges, Opt. Express **13**, 6974–6979 (2005).
[11] M. Castaing, F. Balembois, P. Georges, T. Georges, K. Schaffers, and J. Tassano, Opt. Lett. **33**, 1234–1236 (2008).
[12] Y. F. Lü, X. H. Zhang, J. Xia, R. Chen, G. Y. Jin, J. G. Wang, C. L. Li, and Z. Y. Ma, Laser Phys. Lett. **7**, 343–346 (2010).
[13] J. V. Sandusky and S. R. J. Brueck, IEEE Photon. Technol. Lett. **8**, 313–315 (1996).
[14] J. Chilla, S. Butterworth, A. Zeitschel, J. Charles, A. Caprara, M. Reed, and L. Spinelli, in: Proceedings of the SPIE: Solid State Lasers XIII, San Jose 2004.
[15] Coherent. www.coherent.com.
[16] P. F. Moulton, J. Opt. Soc. Am. B **3**, 125–133 (1986).
[17] S. A. Payne, L. L. Chase, L. K. Smith, W. L. Kway, and H. W. Newkirk, J. Appl. Phys. **66**, 1051–1056 (1989).

[18] W. L. Zhou, Y. Mori, T. Sasaki, S. Nakai, K. Nakano, and S. Niikura, Jpn. J. Appl. Phys. **34**, 3518–3521 (1995).
[19] L. S. Cruz and F. C. Cruz, Opt. Express **15**, 11913–11921 (2007).
[20] F. Falcoz, F. Balembois, P. Georges, and A. Brun, Opt. Lett. **20**, 1274–1276 (1995).
[21] S. Makio, T. Miyai, M. Sato, and T. Sasaki, Jpn. J. Appl. Phys. **39**, 6539–6541 (2000).
[22] A. J. Maclean, P. Roth, G. J. Valentine, A. J. Kemp, and D. Burns, in: Proceedings of Advanced Solid States Photonics (ASSP), Denver, CO, 2009, OSA Technical Digest Series (CD) (Optical Society of America, 2009), paper WE2.
[23] F. Balembois, F. Falcoz, F. Kerboull, F. Druon, P. Georges, and A. Brun, IEEE J. Quantum Electron. **33**, 269–278 (1997).
[24] B. Cocquelin, D. Holleville, G. Lucas-Leclin, I. Sagnes, A. Garnache, M. Myara, and P. Georges, Appl. Phys. B **95**, 315–321 (2009).
[25] S. J. McGinily, R. H. Abram, K. S. Gardner, E. Riis, A. I. Ferguson, and J. S. Roberts, IEEE J. Quantum Electron. **43**, 445–450 (2007).
[26] Y. F. Chen, Y. S. Chen, T. H. Ou, and K. W. Su, Appl. Phys. B **81**, 517–520 (2005).
[27] X. Mu and Y. J. Ding, Opt. Lett. **30**, 1372–1374 (2005).
[28] J. Limpert, H. Zellmer, P. Riedel, G. Maze, and A. Tunnermann, Electron. Lett. **36**, 1386–1387 (1991).
[29] S. Spiekermann and F. Laurell, in: Advanced Solid State Lasers, OSA Technical Digest Series, paper MA10, Optical Society of America, Davos 2000.
[30] Y. Lü, X. Zhang, W. Cheng, and J. Xia, Appl. Opt. **49**, 4096–4099 (2010).
[31] V. Lupei, G. Aka, and D. Vivien, Opt. Lett. **31**, 1064 (2006).
[32] D. Paboeuf, G. Lucas-Leclin, P. Georges, B. Sumpf, G. Erbert, C. Varona, P. Loiseau, G. Aka, and B. Ferrand, Appl. Phys. B **92**, 189–193 (2008).
[33] C. Varona, P. Loiseau, G. Aka, and B. Ferrand, in: Proceedings of Advanced Solid State Photonics, paper WB19, Optical Society of America, Lake Tahoe 2006.
[34] M. Birnbaum, A. W. Tucker, and P. J. Pomphrey Jr, IEEE J. Quantum Electron. **8**, 501 (1972).
[35] C. T. A. Brown, J. Amin, D. P. Shepherd, A. C. Tropper, M. Hempstead, and J. M. Almeida, Opt. Lett. **22**, 1778–1780 (1997).
[36] D. Jaque, J. A. Muñoz, F. Cussó, and J. García Solé, J. Phys., Condens. Matter **10**, 7901 (1998).
[37] F. Mougel, G. Aka, A. Kahn-Harari, H. Hubert, J.-M. Benitez, and D. Vivien, Opt. Mater. **8**, 161 (1997).
[38] M. Castaing, E. Hérault, F. Balembois, P. Georges, C. Varona, P. Loiseau, and G. Aka, Opt. Lett. **32**, 799–801 (2007).
[39] T. Kellner, Ph. D. thesis, Universität Hamburg (1999).
[40] C. Czeranowsky, M. Schmidt, E. Heumann, G. Huber, S. Kutovoi, and Y. Zavartsev, Opt. Commun. **205**, 361–365 (2002).
[41] T. Y. Fan and R. L. Byer, IEEE J. Quantum Electron. **23**, 605 (1987).
[42] W. P. Risk, J. Opt. Soc. Am. B **5**(7), 1412–1423 (1988).
[43] T. Taira, W. M. Tulloch, and R. L. Byer, Appl. Opt. **36**, 1867–1874 (1997).
[44] F. Augé, F. Druon, F. Balembois, P. Georges, A. Brun, F. Mougel, G. Aka, and D. Vivien, IEEE J. Quantum Electron. **36**, 598–606 (2000).
[45] S. Yiou, F. Balembois, and P. Georges, J. Opt. Soc. Am. B **22**(3), 572–581 (2005).
[46] Y. Lü, J. Xia, W. Cheng, J. Chen, G. Ning, and Z. Liang, Opt. Lett. **35**, 3670–3672 (2010).
[47] E. Hérault, F. Balembois, and P. Georges, Opt. Lett. **31** 2731–2733 (2006).
[48] M. Castaing, F. Balembois, and P. Georges, Opt. Lett. **33**, 1957–1959 (2008).
[49] Y. F. Lü, X. H. Zhang, R. Chen, J. Xia, J. F. Chen, and Z. T. Liu, Laser Phys. Lett. **7**, 347–350 (2010).
[50] M. Bass, L. S. Weichman, S. Vigil, and B. K. Brickeen, IEEE J. Quantum Electron. **39**, 741–748 (2003).
[51] http://www.nichia.com.
[52] http://www.kimmon.com.